NIH RELAIS Document Delivery

NIH -- W1 NA81

PAMELA GEHRON ROBEY
CSDB/NIDR/NIH Bldng 30 Rm 228
30 CONVENT DRIVE MSC 4320
BETHESDA, MD   20892

ATTN:		SUBMITTED:	2001-11-19 16:21:26
PHONE: 301-496-4563		PRINTED:	2001-11-20 12:55:16
FAX: 301-402-0824		REQUEST NO.:	NIH-10071778
E-MAIL:		SENT VIA:	LOAN DOC
			5052856

NIH   Fiche to Paper   Journal

TITLE:	NATURE
PUBLISHER/PLACE:	Nature Publishing Group London :
VOLUME/ISSUE/PAGES:	1993 Dec 16;366(6456):654-63 654-63
DATE:	1993
AUTHOR OF ARTICLE:	Noel JP; Hamm HE; Sigler PB;
TITLE OF ARTICLE:	The 2.2 A crystal structure of transducin-alpha co
ISSN:	0028-0836
OTHER NOS/LETTERS:	Library reports holding volume or year
	0410462
	8259210
SOURCE:	PubMed
CALL NUMBER:	W1 NA81
REQUESTER INFO:	AB424
DELIVERY:	E-mail: probey@DIR.NIDCR.NIH.GOV
REPLY:	Mail:

-----National-Institutes-of-Health,-Bethesda,-MD--------------------------

85. Hall, C. et al. J. molec. Biol. **211**, 11–16 (1990).
86. Otsu, M. et al. cell **65**, 91–104 (1991).
87. Skolnik, E. Y. et al. Cell **65**, 83–90 (1991).
88. George, J. M. & Clayton, D. F. Molec. Brain Res. **12**, 323–329 (1992).
89. LeClerc, S. et al. J. biol. Chem. **266**, 17333–17340 (1991).
90. Agnel, M., Roder, L., Vola, C. & Griffin-Shea, R. Molec. cell. Biol. **12**, 5111–5122 (1992).
91. Tan, T., Vollmer, P. & Gallwitz, D. FEBS Lett. **291**, 322–326 (1991).
92. Walsorth, N. C., Brennwald, P., Kabcenell, A. K., Garrett, M. & Novick, P. Molec. cell. Biol. **12**, 2017–2028 (1992).
93. Strom, M., Vollmer, P., Tan, T. J. & Gallwitz, D. Nature **361**, 736–739 (1993).
94. Clarke, S. A. Rev. Biochem. **61**, 355–386 (1992).
95. Schafer, W. R. & Rine, J. A. Rev. Genet. **30**, 209–237 (1992).
96. Boguski, M. S. J. Lipid Res. **33**, 957–974 (1992).
97. Boguski, M. S., Murray, A. W. & Powers, S. New Biologist **4**, 408–411 (1992).
98. Armstrong, S. A., Seabra, M. C., Sudhof, T. C., Goldstein, J. L. & Brown, M. S. J. biol. Chem. **268**, 12221–12229 (1993).
99. Andres, D. A., Goldstein, J. L., Ho, Y. K. & Brown, M. S. J. biol. Chem. **268**, 1383–1390 (1993).
100. Reiss, Y., Brown, M. S. & Goldstein, J. L. J. biol. Chem. **267**, 6403–6408 (1992).
101. Reiss, Y. et al. J. biol. Chem. **266**, 10672–10677 (1991).
102. Ho, B. et al. Proc. natn. Acad. Sci. U.S.A. **88**, 11373–11377 (1991).
103. Gomez, R. et al. Biochem. J. 25–31 (1993).
104. Kohl, N. E. et al. Science **260**, 1934–1937 (1993).
105. James, G. L. et al. Science **260**, 1937–1942 (1993).
106. Mayer, M. L., Caplin, B. E. & Marshall, M. S. J. biol. Chem. **267**, 20589–20593 (1993).
107. Zhang, F. J. biol. Chem. (in the press).
108. Ohya, Y. et al. J. biol. Chem. **266**, 12356–12360 (1991).
109. Seabra, M. C., Goldstein, J. L., Sudhof, T. C. & Brown, M. S. J. biol. Chem. **267**, 14497–14503 (1992).

110. Andres, D. A. et al. Cell **73**, 1091–1099 (1993).
111. Armstrong, S. A., Seabra, M. C., Sudhof, T. C., Goldstein, J. L. & Brown, M. S. J. biol. Chem. **268**, 12221–12229 (1993).
112. Rossi, G., Jiang, Y., Newman, A. P. & Ferro-Novick, S. Nature **351**, 158–161 (1991).
113. Jiang, Y., Rossi, G. & Ferro-Novick, S. Nature **366**, 84–86 (1993).
114. Li, R., Havel, C., Watson, J. A. & Murray, A. W. Nature **366**, 82–84 (1993).
115. Sottleman, J., Albright, C. F., Foster, L. C. & Weinberg, R. A. Nature **350**, 153–154 (1992).
116. McGlade, J. et al. EMBO J. **12**, 3073–3081 (1993).
117. Shou, C., Farnsworth, C. L., Neel, B. G. & Feig, L. A. Nature **358**, 351–354 (1992).
118. Wei, W. et al. Proc. natn. Acad. Sci. U.S.A. **89**, 7100–7104 (1992).
119. Martegani, E. et al. EMBO J. **11**, 2151–2157 (1992).
120. Simon, M. A., Bowtell, D. D. L., Dodson, G. S., Laverty, T. R. & Rubin, G. M. Cell **67**, 701–716 (1991).
121. Bairoch, A. Nucleic Acids Res. **19**, 2241–2245 (1991).
122. Bairoch, A. & Boeckmann, B. Nucleic Acids Res. **20**, 2019–2022 (1992).
123. Kohl, N. E. et al. J. biol. Chem. **266**, 18884–18888 (1991).
124. Boguski, M. S., Love, T. M. J. & Tolstoshev, C. M. Nature Genet. **4**, 332–333 (1993).
125. Schuler, G. D., Altschul, S. F. & Lipman, D. J. Proteins struct. funct. Genet. **9**, 180–190 (1991).
126. Boguski, M. S., Bairoch, A., Attwood, T. K. & Michaels, G. S. Nature **358**, 113 (1992).
127. Hart, M. J. et al. J. biol. Chem. (in the press).
128. Gulbins, E. et al. Science **260**, 822–825 (1993).

ARTICLES

The 2.2 Å crystal structure of transducin-α complexed with GTPγS

Joseph P. Noel[*]**, Heidi E. Hamm**[†‡] **& Paul B. Sigler**[*§]

* Department of Molecular Biophysics and Biochemistry and the Howard Hughes Medical Institute, Yale University, 295 Congress Avenue, Boyer Center for Molecular Medicine, Room 154, New Haven, Connecticut 06510, USA
† Department of Physiology and Biophysics, University of Illinois at Chicago, Chicago, Illinois 60680, USA
‡ Istituto di Fisiologia Generale e Chimica Biologica, Universita' di Sassari, 07100 Sassari, Italy

The 2.2 Å crystal structure of activated rod transducin, $G_{t\alpha} \cdot GTP\gamma S$, shows the bound GTPγS molecule occluded deep in a cleft between a domain structurally homologous to small GTPases and a helical domain unique to heterotrimeric G proteins. The structure, when combined with biochemical and genetic studies, suggests: how an activated receptor might open this cleft to allow nucleotide exchange; a mechanism for GTP-induced changes in effector and receptor binding surfaces; and a mechanism for GTPase activity not evident from previous data.

HERE we describe the three-dimensional structure of the activated α-subunit of a heterotrimeric ($\alpha\beta\gamma$) G protein, namely the complex of transducin-α with the GTP analogue GTPγS. The model and the mechanisms inferred from it were derived from an X-ray crystal structure refined to a resolution of 2.2 Å. The model provides a stereochemical context for the extensive biochemical and mutagenic studies[1] on the highly homologous family of G-protein-coupled signal transduction systems.

Each heterotrimeric G protein is functionally coupled to a specific seven-helix transmembrane receptor, but all share a common mechanism by which information is transduced from the receptor through a GTP-activated α-subunit or a free $\beta\gamma$ heterodimer to specific downstream effectors. GTP's γ-phosphate acts as a molecular switch that relays information in the form of a conformational change. This conformational change leads to a decreased affinity for both the receptor and the $\beta\gamma$ heterodimer,

and an increased specific affinity for and activation of an effector enzyme or channel which ultimately leads to a change in the cellular concentration of a second messenger such as a cyclic nucleotide, Ca^{2+}, inositol phosphates, or diacylglycerol. The released $\beta\gamma$ subunit can itself lead to the activation or modulation of some effectors[2,3]. A GTPase-controlled timing mechanism inherent in all α-subunits and, in some cases, modulated by other proteins[4,5] returns the GTP-activated α-subunit to the inactive GDP-bound heterotrimer.

In the vertebrate light response, inactive heterotrimeric transducin ($G_{t\alpha\beta\gamma} \cdot GDP$) binds the photoactivated rhodopsin (meta-rhodopsin II) and releases GDP. GTP binds firmly to the α-subunit of the receptor-bound transducin causing $G_{t\alpha} \cdot GTP$ to separate from both the receptor and the $\beta\gamma$ heterodimer. The $G_{t\alpha} \cdot GTP$ complex activates its effector, cGMP-specific phosphodiesterase ($\alpha\beta\gamma_2$ cGMP–PDE) by binding to its inhibitory γ-subunit(s).

Activated $\alpha\beta$ cGMP–PDE lowers the concentration of
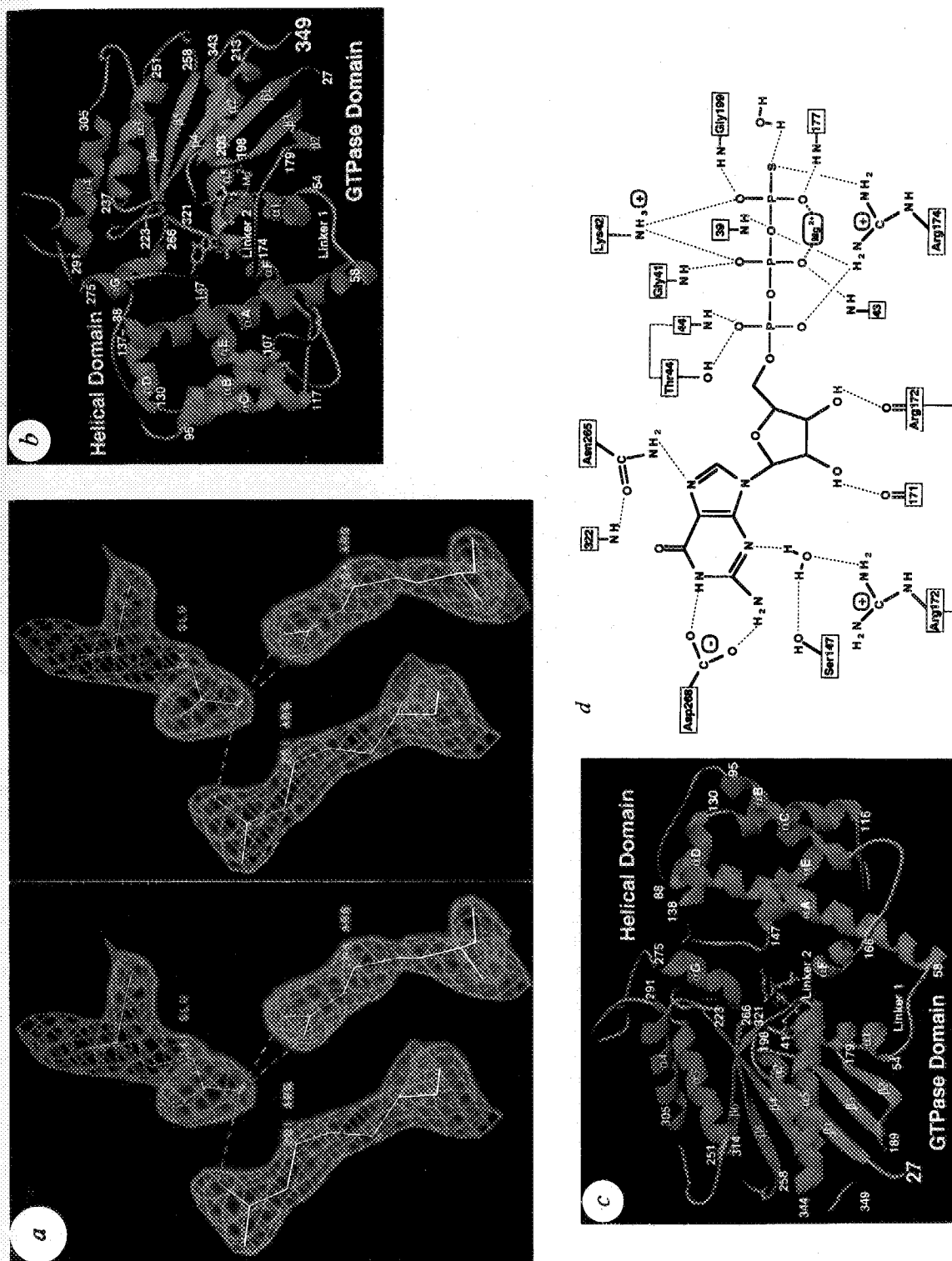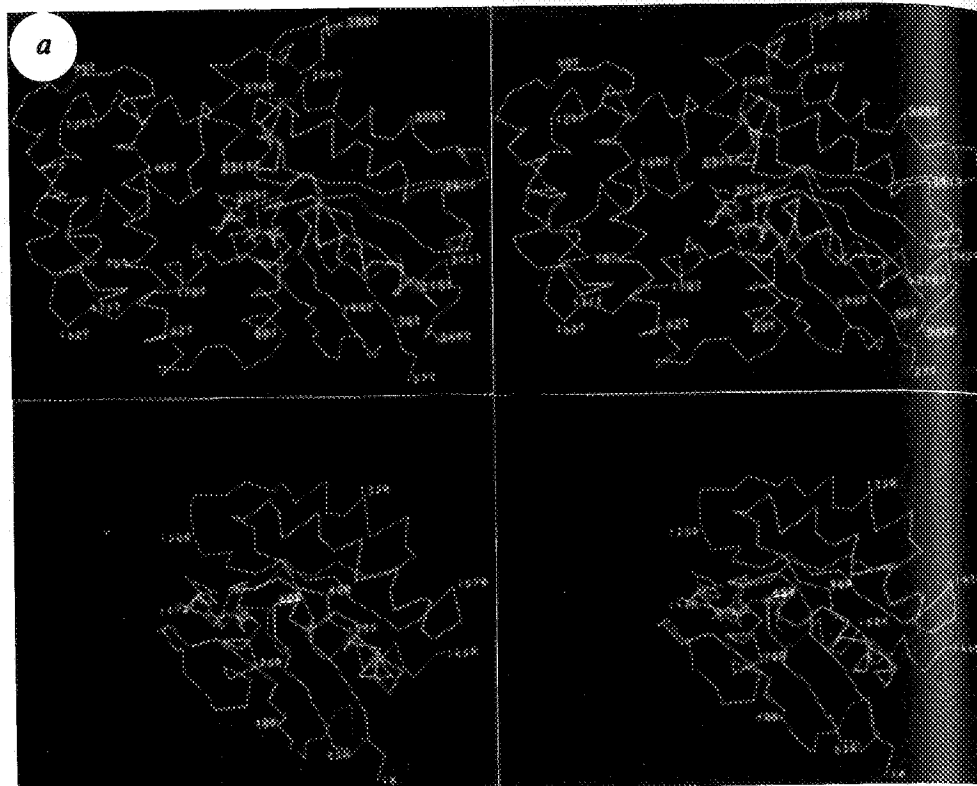
§ To whom correspondence should be addressed.

FIG. 1 The overall structure of (.25)G$_{t\alpha}$·GTPγS. a, Representative electron density. The map was calculated at 2.2 Å resolution with (2F$_o$−F$_c$) amplitudes and model phases and is contoured at 2.0σ. This example illustrates electrostatic linkages that convey the signal to the effector binding region (see Fig. 4a, b, c for details.) b, Ribbon drawing (Ribbons[43]). The γ-phosphate appears yellow while the rest of the nucleotide is lavender. The catalytically essential Mg^{2+} is represented as a cyan sphere. For clarity, labels for the secondary structural elements of the core GTPase domain reflect the convention used to describe Ras[17]. The seven additional helices which are unique in the G$_{t\alpha}$·GTPγS structure are labelled A through G. Although the crystallized construct spans residues 26 through 350, the crystallographically observable N and C termini are Ala 27 and Leu 349. c, Alternative view of the overall fold of the complex rotated 170° around a vertical axis from the view in (b). d, Schematic illustration of the major interactions securing GTPγS in the nucleotide binding cleft. Hydrogen bonds are denoted by dashed lines. Only the interactions observed in all three complexes are shown. All of the figures were constructed from the coordinates of one of the complexes, but they are representative of the other two. (The r.m.s. deviation of all atoms for protomer pairs is 1.14 Å for protomer A to B, 0.95 Å for protomer A to C and 1.03 Å for protomer B to C. The r.m.s. deviation for backbone atoms only is 0.50 Å for A to B, 0.42 Å for A to C and 0.44 Å for B to C.)

655

FIG. 2 Primary and tertiary structural alignment of (-25)$G_{t\alpha}$·GTPγS with representative GTPases. a, Stereoview of the α carbon trace and bound nucleotides for $G_{t\alpha}$·GTPγS and Ras·GMP.PNP[12] in the same orientation. $G_{t\alpha}$·GTPγS appears in light blue and residue numbers are appended with T. Ras·GMP.PNP appears in pink and its sequence numbers are appended with R. The root mean square difference in backbone positions (excluding surface loops) between the GTPase domains of $G_{t\alpha}$ and Ras–GMP.PNP[12] is 1.85 Å. b, Primary sequence alignment. The observed secondary structural elements as deduced from $G_{t\alpha}$ are indicated below the sequences. The location of functional domains are indicated above the sequences as are the sequence numbers for $G_{t\alpha}$. Regions considered as 'inserts' in the GTPase domain are included above the aligned sequences. The amino acids are donoted by their one letter codes. Gaps in the aligned sequences are indicated by dots. Sources of sequence information: bovine $G_{s\alpha}$[44], bovine $G_{i\alpha}$[45]. bovine $G_{o\alpha}$[46], mouse $G_{q\alpha}$[47], bovine $G_{z\alpha}$[48], bovine rod $G_{t\alpha}$[49], Ras[50], E. coli EF-Tu[51].

cGMP, which closes cGMP-gated cation channels and hyperpolarizes the retinal rod cell, thereby generating the nerve impulse. $G_{t\alpha}$·GDP releases PDE-γ leading to a reformation of both the inactive cGMP–PDE $\alpha\beta\gamma_2$ complex and the inactive $G_{t\alpha\beta\gamma}$·GDP heterotrimer which is primed for reactivation by metarhodopsin II (refs 6–8).

Structure determination and refinement

A 325-amino-acid fragment of bovine retinal rod cell $G_{t\alpha}$·GTPγS lacking residues 1–25 was obtained by proteolysis of the full-length GTPγS complex with endoproteinase lysC (ref. 9). Although the removal of the N terminus results in a loss of βγ binding, the GTPγS complex fully retains its capacity to activate its target enzyme cGMP–PDE. The best crystals (space group P2₁) were grown at -12.5 °C in high concentrations of cacodylate buffer and CaCl₂ and contained three complexes per asymmetric unit. Phases from two heavy-atom derivatives of marginal quality were substantially improved by a solvent-flattening procedure employing maximum entropy routines (Z. Otwinowski) and subsequent averaging of the non-crystallographically related density in the asymmetric unit (Table 1).

A model for each of the three non-crystallographically related complexes was built into the final averaged map with the program FRODO (ref. 10) and refined with XPLOR 3.1 (ref. 11) to an R-factor of 19.0% for all data, and 17.8% for data greater than 2σ between 6.0 and 2.2 Å resolution. The free R-factor for a randomly omitted subset (10%) of data (no cut-off) was 30.4 and 28.7% for data greater than 2.0σ. The average deviation from standard values is 0.011 Å in bond distance and 1.8° in bond angle; the Φ–Ψ plot showed all residues except for Asn 54 and some glycines within 10° of the allowed regions. A representative segmet of the unaveraged electron density map is shown in Fig. 1a.
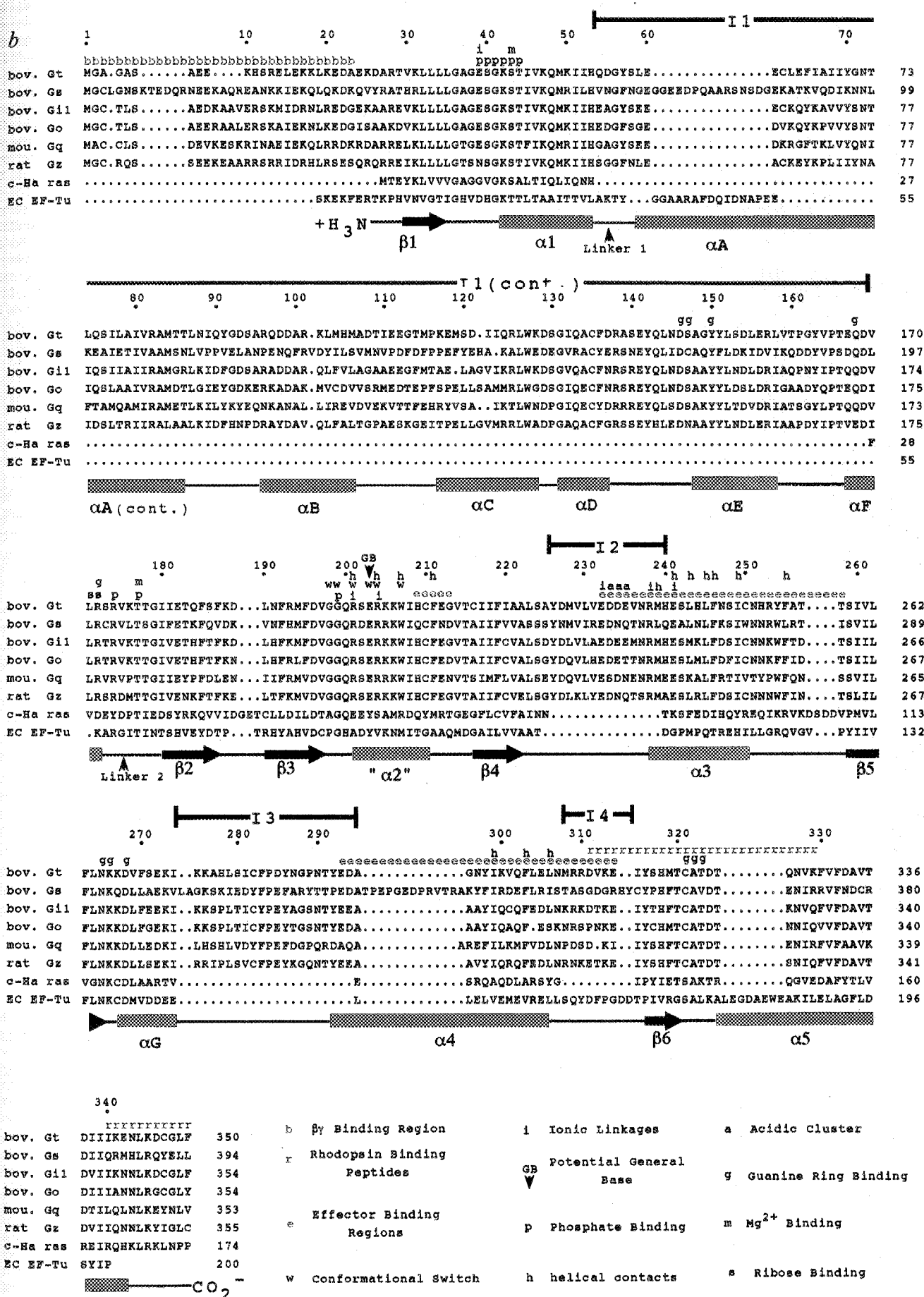
The domain architecture

The (-25)$G_{t\alpha}$·GTPγS complex consists of two easily delineated domains (Fig. 1b and c) flanking a deep guanine-nucleotide-binding cleft (Fig. 1d). One domain is a highly conserved GTPase domain that is structurally similar to the αβ fold of the c-H-ras protein, p21^{Ha-ras} or Ras[12] (Fig. 2a), even though the sequence indentity is low (19.0%; Fig. 2b). This domain, also seen in the protein synthesis elongation factor EF-Tu (ref. 13), consists of a six-stranded β-sheet (β1–β6) surrounded by a set of five helices (α1–α5). The other domain is a highly helical domain unique to heterotrimeric G proteins. Altogether, there are four dfferences between the (-25)$G_{t\alpha}$·GTPγS complex and a consensus GTPase fold as represented by Ras: one is the large helical domain just mentioned (I1); the other three occur as sequence insertions within loops of the GTPase domain (I2, I3, I4).

The highly helical domain (I1) spans residues 59–172 (Fig. 2b). It is connected to the GTPase domain by two polypeptide segments, hereafter referred to as linker 1 and linker 2. Linker 1, spanning residues 54–58, follows α1. Linker 2, spanning residues 173–179, immediately precedes β2. The helical domain and the GTPase domain clamp down upon and completely bury the GTPγS molecule and its associated Mg²⁺ ion. EF-Tu (refs 13–15) and the smaller GTPase, Ras[12], which both lack this helical domain, bind the nucleotide in a partially exposed surface cleft. The inaccessibility of GTPγS in $G_{t\alpha}$ suggests that in order to exchange guanine nucleotides there must be a conformational change that opens the cleft. The helical domain encompasses a central α-helical scaffold of 28 residues which supports five smaller helices through hydrophobic interactions. The seemingly rigid internal structure of the helical domain suggests that conformational changes in the linkers would be amplified into 'en bloc' movements of the helical domain, making it a lid on the nucleotide binding site.

Insert I2 residues between β4 and α3 and makes critical ionic contacts to both the conserved phosphate-binding loop[16] and the so-called switch II region[17], residues 198–215. We will invoke these interactions when we consider a mechanism for the propagation of a conformational change from the γ-phosphate binding region to the effector (PDE-γ) binding loops. The third

656

b

```
        1              10            20            30            40            50            60            70
                                                                                    ⊢━━━━━━━ I 1 ━━━━━━━━━━
        bbbbbbbbbbbbbbbbbbbbbbbbbbbbbbbbbbbbb                 ppppppp
                                                              i  m
bov. Gt  MGA.GAS......AEE....KHSRELEKKLKEDAEKDARTVKLLLLGAGESGKSTIVKQMKIIHQDGYSLE..............ECLEFIAIIYGNT   73
bov. Gs  MGCLGNSKTEDQRNEEKAQREANKKIEKQLQKDKQVYRATHRLLLLGAGESGKSTIVKQMRILEVNGFNGEGGEEDPQAARSNSDGEKATKVQDIKNNL  99
bov. Gi1 MGC.TLS......AEDKAAVERSKMIDRNLREDGEKAAREVKLLLLGAGESGKSTIVKQMKIIHEAGYSEE..............ECKQYKAVVYSNT   77
bov. Go  MGC.TLS......AEERAALERSKAIEKNLKEDGISAAKDVKLLLLGAGESGKSTIVKQMKIIHEDGFSGE..............DVKQYKPVVYSNT   77
mou. Gq  MAC.CLS......DEVKESKRINAEIEKQLRRDKRDARELKLLLLGTGESGKSTFIKQMRIIHGAGYSEE..............DKRGFTKLVYQNI   77
rat  Gz  MGC.RQS......SEEKEAARRSRRIDRHLRSESQRQRREIKLLLLGTSNSGKSTIVKQMKIIHSGGFNLE..............ACKEYKPLIIYNA   77
c-Ha ras .................................MTEYKLVVVGAGGVGKSALTIQLIQNH.........................................   27
EC EF-Tu .....................SKEKFERTKPHVNVGTIGHVDHGKTTLTAAITTVLAKTY...GGAARAFDQIDNAPEE..................   55
```

+H₃N β1 α1 Linker 1 αA

```
                 ⊢━━━━━━━━━━━━━━━━━━━━━━━━ T 1 ( con⁺. ) ━━━━━━━━━━━━━━━━━━━━━━━━━━━┤
        80        90        100       110       120       130       140       150       160
                                                                          gg  g                    g
bov. Gt  LQSILAIVRAMTTLNIQYGDSARQDDAR.KLMHHMADTIEEGTMPKEMSD.IIQRLWKDSGIQACFDRASEYQLNDSAGYYLSDLERLVTPGYVPTEQDV  170
bov. Gs  KEAIETIVAAMSNLVPPVELANPENQFRVDYILSVMNVPDFDFPPEFYEHA.KALWEDEGVRACYERSNEYQLIDCAQYFLDKIDVIKQDDYVPSDQDL  197
bov. Gi1 IQSIIAIIRAMGRLKIDFGDSARADDAR.QLFVLAGAAEEGFMTAE.LAGVIKRLWKDSGVQACFNRSREYQLNDSAAYYLNDLDRIAQPNYIPTQQDV  174
bov. Go  IQSLAAIVRAMDTLGIEYGDKERKADAK.MVCDVVSRMEDTEPFSPELLSAMMRLWGDSGIQECFNRSREYQLNDSAKYYLDSLDRIGAADYQPTEQDI  175
mou. Gq  FTAMQAMIRAMETLKILYKYEQNKANAL.LIREVDVEKVTTFEHRYVSA..IKTLWNDPGIQECYDRRREYQLSDSAKYYLTDVDRIATSGYLPTQQDV  173
rat  Gz  IDSLTRIIRALAALKIDFHNPDRAYDAV.QLFALTGPAESKGEITPELLGVMRRLWADPGAQACFGRSSEYHLEDNAAYYLNDLERIAAPDYIPTVEDI  175
c-Ha ras .....................................................................................................F   28
EC EF-Tu ..................................................................................................... 55
```

αA(cont.) αB αC αD αE αF

```
                        180       190       200 GB   210       220       230       240       250       260
              g   m                         ▽
             ss  p   p                       h  h  h       h                              h  hh  h       h
                                            *h     *h*h                                   *h    *h*     *
                                            ww    w  ww                                   iaaa   ih  i
                                              w                eeeee                          eeeeeeeeeeeeeeeeeeeeeeeeeee
                                                                  ⊢━━ I 2 ━━┤
bov. Gt  LRSRVKTTGIIETQFSFKD...LNFRMFDVGGQRSERKKWIHCFEGVTCIIFIAALSAYDMVLVEDDEVNRMHESLHLFNSICNHRYFAT....TSIVL  262
bov. Gs  LRCRVLTSGIFETKFQVDK...VNFHMFDVGGQRDERRKWIQCFNDVTAIIFVVASSGYNMVIREDNQTNRLQEALNLFKSIWNNRWLRT....ISVIL  289
bov. Gi1 LRTRVKTTGIVETHFTFKD...LHFKMFDVGGQRSERKKWIHCFEGVTAIIFCVALSDYDLVLAEDEEMNRMHESMKLFDSICNNKWFTD....TSIIL  266
bov. Go  LRTRVKTTGIVETHFTFKN...LHFRLFDVGGQRSERKKWIHCFEDVTAIIFCVALSGYDQVLHEDETTNRMHESLMLFDFICNNKFFID....TSIIL  267
mou. Gq  LRVRVPTTGIIEYPFDLEN...IIFRMVDVGGQRSERKKWIHCFENVTSIMFLVALSEYDQVLVESDNENRMEESKALFRTIVTYPWFQN....SSVIL  265
rat  Gz  LRSRDMTTGIVENKFTFKE...LTFKMVDVGGQRSERKKWIHCFEGVTAIIFCVELSGYDLKLYEDNQTSRMAESLRLFDSICNNNWFIN....TSLIL  267
c-Ha ras VDEYDPTIEDSYRKQVVIDGETCLLDILDTAGQEEYSAMRDQYMRTGEGFLCVFAINN..............TKSFEDIHQYREQIKRVKDSDDVPMVL  113
EC EF-Tu .KARGITINTSHVEYDTP...TREYAHVDCPGHADYVKNMITGAAQMDGAILVVAAT..............DGPMPQTREHILLGRQVGV...PYIIV  132
```

Linker 2 β2 β3 "α2" β4 α3 β5

```
              ⊢━━ I 3 ━━┤                              ⊢ I 4 ┤
           270       280       290       300       310       320       330
          gg  g                          h  h  h      rrrrrrrrrrrrrrrrrrrrrrrrrrrrr
                          eeeeeeeeeeeeeeeeeeeeeeeeeeeeeeeeeeee          ggg
bov. Gt  FLNKKDVFSEKI..KKAHLSICFPDYNGPNTYEDA...........GNYIKVQFLELNMRRDVKE..IYSHMTCATDT.......QNVKFVFDAVT  336
bov. Gs  FLNKQDLLAEKVLAGKSKIEDYFPEFARYTTPEDATPEPGEDPRVTRAKYFIRDEFLRISTASGDGRHYCYPHFTCAVDT.......ENIRRVFNDCR  380
bov. Gi1 FLNKKDLFEEKI..KKSPLTICYPEYAGSNTYEEA...........AAYIQCQFEDLNKRKDTKE..IYTHFTCATDT.......KNVQFVFDAVT  340
bov. Go  FLNKKDLFGEKI..KKSPLTICFPEYTGSNTYEDA...........AAYIQAQF.ESKNRSPNKE..IYCHMTCATDT.......NNIQVVFDAVT  340
mou. Gq  FLNKKDLLEEKI..LHSHLVDYFPEFDGPQRDAQA...........AREFILKMFVDLNPDSD.KI..IYSHFTCATDT.......ENIRFVFAAVK  339
rat  Gz  FLNKKDLLSEKI..RRIPLSVCFPEYKGQNTYEEA...........AVYIQRQFEDLNRNKETKE..IYSHFTCATDT.......SNIQFVFDAVT  341
c-Ha ras VGNKCDLAARTV...................E...........SRQAQDLARSYG.........IPYIETSAKTR.......QGVEDAFYTLV  160
EC EF-Tu FLNKCDMVDDEE...................L...........LELVEMEVRELLSQYDFPGDDTPIVRGSALKALEGDAEWEAKILELAGFLD  196
```

αG α4 β6 α5

```
        340
        rrrrrrrrrrr
bov. Gt  DIIIKENLRDCGLF  350
bov. Gs  DIIQRMHLRQYELL  394
bov. Gi1 DVIIKNNLRDCGLF  354
bov. Go  DIIIANNLRGCGLY  354
mou. Gq  DTILQLNLKEYNLV  353
rat  Gz  DVIIQNNLKYIGLC  355
c-Ha ras REIRQHKLRKLNPP  174
EC EF-Tu SYIP          200
```

▨━━━━━━CO₂⁻

b	βγ Binding Region	i	Ionic Linkages	a	Acidic Cluster
r	Rhodopsin Binding Peptides	GB ▽	Potential General Base	g	Guanine Ring Binding
e	Effector Binding Regions	p	Phosphate Binding	m	Mg²⁺ Binding
w	Conformational Switch	h	helical contacts	s	Ribose Binding

(left margin fragments)
...nserved of the ...gh the ...n, also ...ef. 13), ...y a set ...helical , there ...ex and e large ...cur as (I2, I3, 2 (Fig. ...eptide ...nker 1, ...esidues ...nd the ...ry the ...efs 13– ...helical e cleft. ...der to ...ational ...asses a ...ts five ...mingly ...t con- ...to 'en ...on the l ionic ...¹⁶ and ...nvoke ...ropa- ...sphate e third 1993
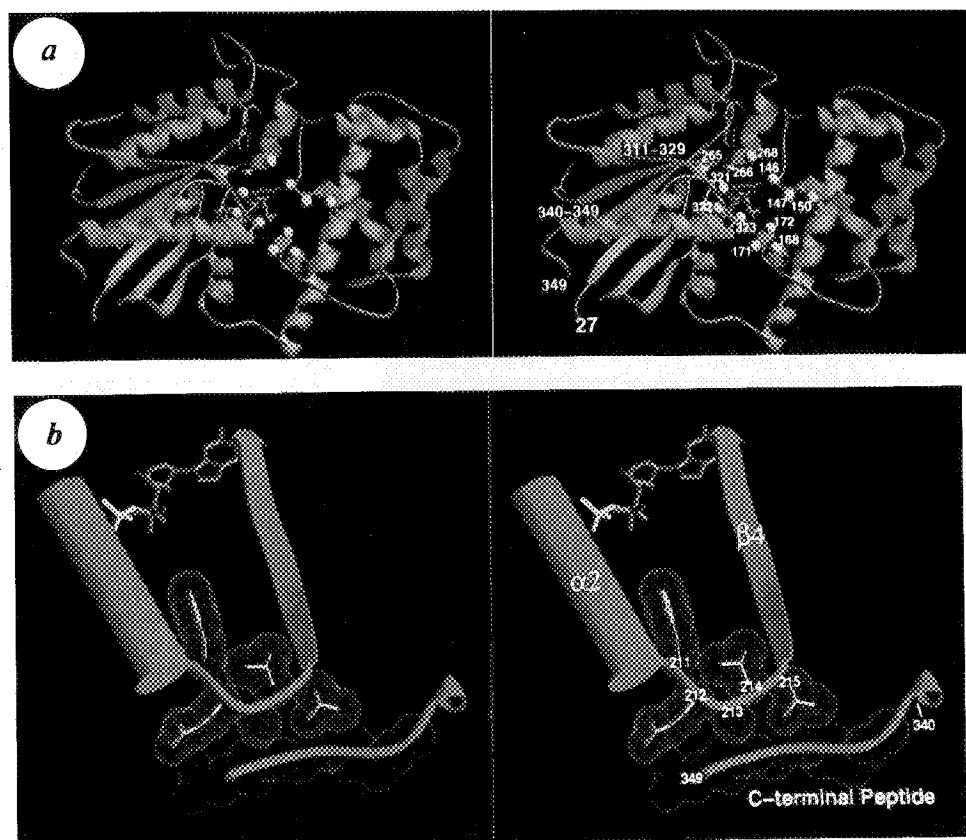
FIG. 3 Linkage between nucleoside binding sites and the receptor interaction surface. *a*, Stereoview of the proposed receptor binding face of G$_{t\alpha}$. Regions involved in receptor binding, 311–329 and 340–350 (ref. 19), and segments participating in nucleoside binding are coloured in light blue. The yellow spheres denote relevant contacts, direct or supporting, to the nucleoside. *b*, Stereoview of the van der Waals contact surface formed between the GTP regulated $\alpha 2/\beta 4$ loop side chains and the backbone of the rhodopsin binding C-terminal peptide. The C-terminal backbone depicted (light blue) spans residues 340–349 while the van der Waals surface of this backbone (red dot surface) encompasses residues 343 to 349. *c*, Stereoview of the cluster of residues highlighted as yellow spheres in *a*. Cys 321 fixes the side chain of Thr 323 which forms a favourable van der Waals surface with the guanine ring. Ala 322's backbone amide positions the side chain of Asn 265 which, in turn, donates a hydrogen bond to the N7 nitrogen of the base. Asp 268 accepts hydrogen bonds from the N1 and N2 nitrogens of guanine. Lys 266 provides a second van der
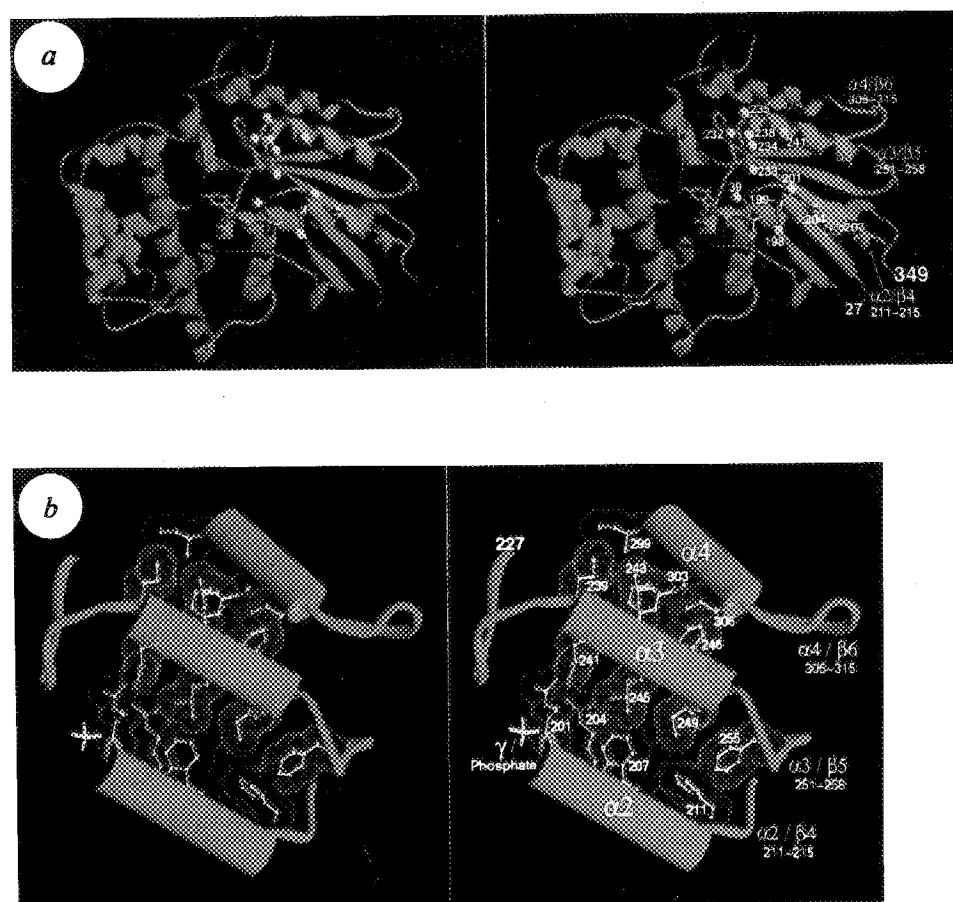
FIG. 4 Linkage between γ-phosphate binding and effector interaction surfaces. *a*, Stereoview highlighting in light blue regions involved in the functional coupling between GTP binding (peptide Gly 198/Gly 199) and the effector binding surfaces ($\alpha 2/\beta 4$, $\alpha 3/\beta 5$, $\alpha 4/\beta 6$) mediated through $\alpha 2$, $\alpha 3$ and $\alpha 4$. In addition, a fourth region comprising an acidic cluster of residues, Glu 232, Asp 233, Asp 234 and Glu 235 is shown and comprises a fourth effector binding surface (J. Mills *et al.*, in preparation). In addition to the acidic cluster, the yellow spheres emphasize specific contacts between the

Waals surface for the guanine ring and is locked in place by the side chain carboxylate of Asp 146 of the helical domain. Both the 2' and 3' ribose hydroxyls donate hydrogen bonds to the backbone carbonyls of residues 171 and 172. The N3 of the guanine ring participates in a water mediated contact fixed in place by the side chains of Ser 147 and Arg 172. Gln 168 and Tyr 150 (not shown) buttress the side chain of Arg 172 through hydrogen bonds and van der Waals forces, respectively. The nucleoside bonds are filled and the protein's backbone bonds are partially filled. Hydrogen bonds are represented by broken bonds. C atoms are black, N, P and S atoms are partially filled and O atoms are white.
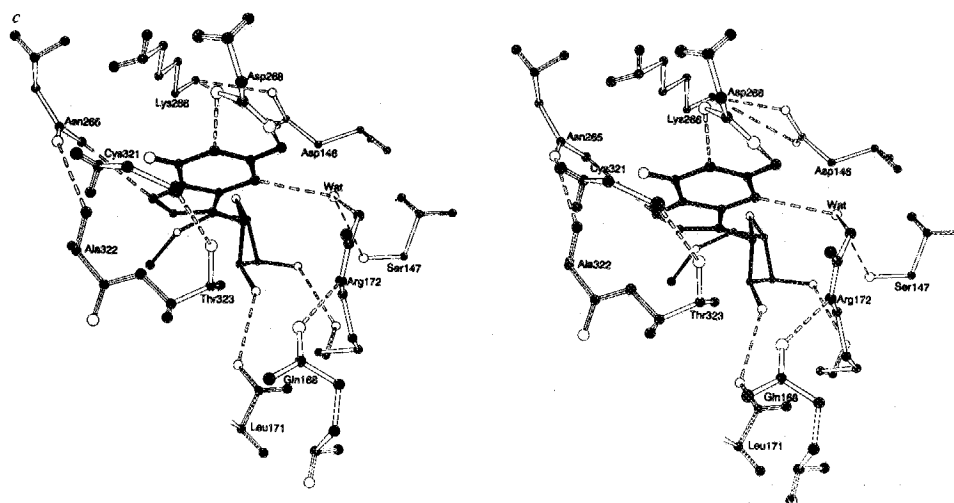
major insert, I3, is situated between $\beta5$ and $\alpha4$ and encompasses αG. The fourth, I4, is a small insert from residues 309 to 314 connecting $\alpha4$ and $\beta6$ and plays a key role in effector recognition.

Guanine-nucleotide binding

Triphosphate binding. The triphosphate portion of GTPγS coordinates an essential Mg^{2+} ion and accepts hydrogen bonds from the backbone amides of Glu 39, Gly 41, Lys 42, Ser 43, Thr 177 and Gly 199, and the side chains of Lys 42 and Arg 174. The Mg^{2+} ion is coordinated in an octahedral arrangement in which two ligands are non-bridging oxygens of the β- and γ-phosphates, two ligands are the side-chain hydroxyl groups of Ser 43 and Thr 177, and two opposing ligands are water molecules that are secured by hydrogen bonds to the side chains of Ser 43, Thr 177 and Asp 196, and a non-bridging oxygen on the α-phosphate.

The binding of the backbone amides of Ser 43 and Thr 177 to the β- and γ-phosphates positions the side chains to interact with the Mg^{2+} ion and with its associated water ligands. The side chain of Arg 174, which is the site for GTPase inhibiting ADP-ribosylation by cholera toxin[18], is hydrogen-bonded to the γ-thiophosphate's sulphur, the bridging oxygen between the β- and γ-phosphate, and a non-bridging oxygen on the α-phosphate (Fig. 1d).

Nucleoside binding. The 2' and 3' hydroxyls of the sugar donate hydrogen bonds to the backbone carbonyls of Leu 171 and Arg 172 in αF. The guanine ring is bound by an interaction that

is unique to the $G_{t\alpha}$ structure, in which the N3 ring nitrogen forms water-mediated interactions with the side chains of Ser 147 and Arg 172. It is noteworthy that the nucleoside contacts (Ser 147, Leu 171 and Arg 172) and the phosphate contacts (Arg 174 and Thr 177) arise from either the helical domain or linker 2, which, as will be discussed in a later section, has important implications for receptor-regulated nucleotide exchange. In addition to these guanine interactions that are unique to G proteins, a series of interactions conserved in the GTPase superfamily further stabilizes the guanine base through hydrogen bonds from side chains of Asn 265 to the N7 ring nitrogen and Asp 268 to the N1 ring nitrogen and exocyclic 2-amine (Fig. 1d). Finally, the guanine ring is sandwiched by van der Waals contacts between the methylene carbons of Lys 266 and the methyl group of Thr 323. Lys 266 is well stabilized by a salt bridge to Asp 146 of the helical domain, and Thr 323 is also locked in place by a supporting hydrogen bond with the side chain of Cys 321. A mechanistically important feature of this system is the elegant manner in which interactions with one portion of the nucleotide support contacts with another. It is likely that these tightly coupled interactions potentiate a highly cooperative receptor-mediated disassembly of the elements that so strongly secure GDP and GTP in the nucleotide-binding cleft.

Rhodopsin binding and nucleotide exchange

The C-terminal receptor-binding site. A peptide designed to mimic the C-terminal 11 residues of $G_{t\alpha}$ not only competes with $G_{t\alpha\beta\gamma}$ binding to photoactivated rhodopsin, but stabilizes rho-

phosphate binding loop (Glu 39), the $\alpha2$ switch region (Gly 198–Trp 207), and the acidic loop (Glu 232–Glu 241). b, Stereoview of the $\alpha2/\alpha3/\alpha4$ interface. The dot surface (van der Waals) emphasizes the stereochemical coupling between the conformationally regulated $\alpha2$ helix and $\alpha3$ and $\alpha4$. c, Detailed stereochemical view of the coupling between the γ-phosphate binding region (Glu 39, Gly 198 and Gly 199), the conformationally regulated $\alpha2$ helix (Arg 201, Arg 204 and Trp 207) and the I2 loop (Glu 232, Arg 238 and Glu 241).
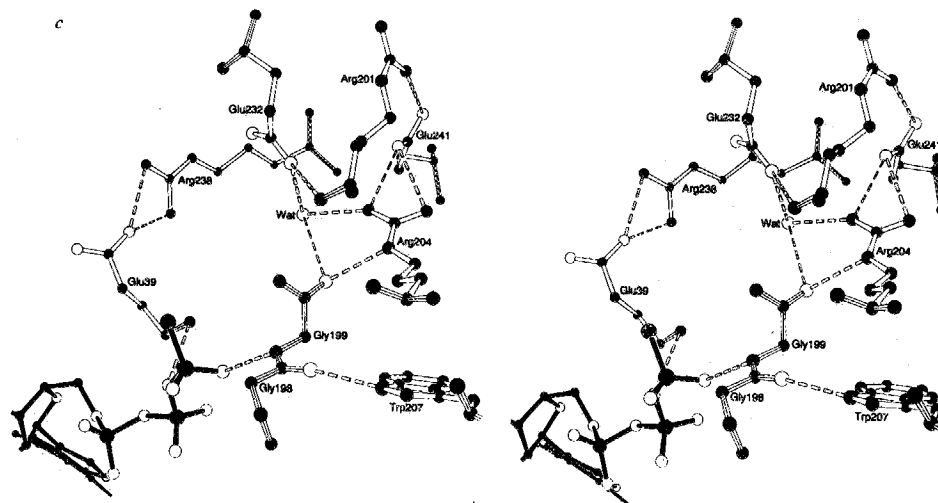
659

TABLE 1 Experimental data on crystal structure determination and refinement

Quality of MIR phases

Resolution limit (Å)	12.6	8.4	6.3	5.0	4.2	3.6	3.2	2.8	Total
CH_3-Hg(OOC.CH_3)$_2$									
Number of reflections	280	760	1,478	2,404	3,571	4,893	3,869	—	17,255
Phasing power	2.53	2.29	2.49	2.05	1.33	1.19	1.37	—	1.49
$SmCl_2$									
Number of reflections	242	758	1,477	2,405	3,573	4,946	6,612	8,264	28,277
Phasing power	2.05	1.04	1.03	0.78	0.47	0.36	0.33	0.31	0.49
Mean figure of merit	0.76	0.79	0.74	0.67	0.55	0.45	0.33	0.19	0.41

Native data and refinement

Resolution limit (Å)	5.41	3.76	3.17	2.84	2.61	2.44	2.31	2.20	Total
Number of reflections	3,977	7,834	7,853	7,803	7,655	7,507	6,101	4,559	53,289
Predicted	4,019	7,839	7,863	7,835	7,820	7,801	7,763	7,792	58,732
R_{sym}	0.026	0.029	0.037	0.049	0.067	0.094	0.108	0.135	0.039
R-factor (all data)	0.173	0.121	0.157	0.205	0.246	0.277	0.304	0.330	0.190
R-factor ($>2.0\sigma$)	0.172	0.121	0.155	0.197	0.231	0.248	0.255	0.268	0.178
Free R-factor (all data)									0.304
Free R-factor ($>2.0\sigma$)									0.287

$R_{sym} = \sum_h \langle |I_{h'} - I_h| \rangle / \sum_h I_h$ where $\langle |I_h - I_h| \rangle$ is the average absolute deviation of reflections I_h from the average $I_{h'}$ of its symmetry and Friedel related equivalents. Phasing power is $\sum |F_h^c| / [|| F_p^o | \exp(i\Phi_c) + F_h^c | - | F_{ph}^o |]$, where F_h^c = heavy atom structure factor and $|F_p^o|$ and $|F_{ph}^o|$ are observed amplitudes for the protein and heavy-atom derivative, respectively, Φ_c is the calculated phase, and the sum is over all observations. Figure of merit is $\int P(\Phi) \exp(i\Phi) d\Phi / \int P(\Phi) d\Phi$, where P is the probability distribution of Φ, the phase angle. $G_{t\alpha}\cdot GTP\gamma S$ was purified from photolysed bovine rod outer segments (ROS) by selective extraction with GTPγS and Mg^{2+} as described[9]. (-25)$G_{t\alpha}\cdot GTP\gamma S$, residues 26–350, was prepared from full-length $G_{t\alpha}\cdot GTP\gamma S$ by overnight proteolysis with endoproteinase LysC (Boehringer Mannheim) at 4 °C in 20 mM Tris-HCl, pH 7.5, 5 mM $MgCl_2$, 1 mM dithiothreitol (DTT) and purified on a Mono-Q (Pharmacia) column with a gradient of 0–225 mM NaCl in 20 mM Tris-HCl, pH 7.5, 0.5 mM DTT. The fractions containing $G_{t\alpha}\cdot GTP\gamma S$ were concentrated and stored at -80 °C in 5 mM Tris-HCl, pH 7.5, 10 mM $MgCl_2$, 25 mM β-mercaptoethanol, 40% (v/v) glycerol at ~40 mg ml^{-1}. The purified protein produced a single band on an overloaded silver-stained denaturing SDS gel and the N-terminal sequence was verified by electroblotting on to polyvinylidene fluoride (Millipore) membrane and sequenced (K. Stone, HHMI, Yale University). Diffraction quality crystals were grown at -12.5 °C from microseeded hanging drops (3–5 μl) containing 20–25 mg ml^{-1} protein, 166 mM sodium cacodylate buffer, pH 6.0, 223 mM $CaCl_2$, 25 mM β-mercaptoethanol, 20% (v/v) glycerol, 3.33% (w/v) PEG 8000 over reservoirs of 5% (w/v) PEG 8000, 250 mM sodium cacodylate buffer, pH 6.0, 350 mM $CaCl_2$, 25 mM β-mercaptoethanol, 30% (v/v) glycerol. Crystals appeared overnight and grew typically to 0.1 mm × 0.1 mm × 0.2 mm over several weeks. They were stabilized at 4 °C in 15% (w/v) PEG 8000, 50 mM sodium cacodylate buffer, pH 6.0, 25 mM β-mercaptoethanol, 30% (v/v) glycerol. The crystals belong to space group P2$_1$ with a = 74.5 Å, b = 108.3 Å, c = 79.0 Å, β = 112.3°. The Sm^{2+} and CH_3-Hg^+ derivative crystals were equilibrated with the stabilizer containing 10 mM $SmCl_2$ or 0.05 mM methyl mercuric acetate (no β-mercaptoethanol), respectively. Parent data and the Sm^{2+} derivative data were each collected from single quick-frozen crystals (-150 °C) on the RAXIS II, processed with DENZO (Z. Otwinowski), and scaled with SCALEPACK (Z. Otwinowski). The CH_3-Hg^+ derivative data were collected on a Siemens Xentronics area detector, processed with XDS[38,39], and scaled with SCALEPACK. The parent and derivative data sets were placed on the same relative scale with SCALEPACK. Heavy-atom positions were determined initially from a combination of isomorphous and anomalous difference Patterson maps, improved with cross-difference Fourier maps, and refined with ML-PHARE[40]. A total of 21 Sm sites and 12 CH_3-Hg sites were located in the asymmetric unit. The MIR phases were improved sequentially by solvent flattening employing maximum entropy routines (Z. Otwinowski) and non-crystallographic averaging with the program SQUASH[41]. The initial superimposition matrices relating the three (-25)$G_{t\alpha}\cdot GTP\gamma S$'s complexes were determined from the positions of the three triphosphates fit from the MIR map and three CH_3-Hg^+ binding sites and refined in SQUASH. The three complexes are related by an approximate 3$_1$ screw axis. The averaging envelope encompassing one of the complexes was constructed manually by filling a clearly delineated protomer with a set of randomly placed dummy atoms with FRODO[10] and converted into the CCP4 map format with ATOMSTOMASK (J. Friedman). A nearly complete model for each of the three non-crystallographically related complexes was built into the final averaged map with FRODO and refined by simulated annealing with XPLOR 3.1 (ref. 11) starting at 4,000 K (0.3 fs time step). The non-crystallographic symmetry was loosely restrained during the first two rounds of refinement at 2.8 Å and 2.5 Å resolution. Local errors were corrected with the aid of the original experimentally phased maps and model phased (2Fo−Fc) and (Fo−Fc) maps. All three models were then refined at 2.2 Å with tightly restrained neighbouring B-factors (r.m.s. deviations in B-factor between bonded atoms is 1.75 Å^2) and no local symmetry restraints. Water sites were gradually and systematically added to the structure with the aid of suitably contoured (Fo−Fc) maps during the later stages of refinement and accepted if they (1) reappeared with strong density in (2Fo−Fc) maps, (2) participated in at least one hydrogen-bonded interaction, and (3) refined to an isotropic B-factor of no more than 70 Å^2 with unit occupancy. The free R-factor[42] consistently decreased throughout the refinement. The current model lacks the N-terminal Asp 26 for all three complexes, residues 343–350 in two of the complexes, and Phe 350 in the third. In addition to the polypeptide backbone, the current model contains three GTPγS molecules, three Mg^{2+} ions, six cacodylate-modified cysteines (Cys 61 and Cys 210) modelled as single As atoms and 826 solvent molecules modelled as water.

dopsin's active Meta II photochemical state[19] (50% inhibitory concentration, IC_{50} = 0.04 mM[20]). In addition, work with $G_{i\alpha}$/$G_{q\alpha}$ chimaeras has established a critical role for the C terminus in specifying the α-subunit's binding to its cognate receptor[21]. Finally, antibodies against the C terminus of G_α (ref. 22), and ADP-ribosylation by pertussis toxin of a cysteine side chain[23,24] four residues from the C terminus, uncouple many G proteins from their receptors. In two of the molecules represented in the asymmetric unit, the final eight residues are somewhat disordered. In a third complex, the C-terminal residues 343–349 of $G_{t\alpha}$ can be seen to make van der Waals contacts with the $\alpha 2$/$\beta 4$ loop, residues 212–215 (Fig. 3a and b). This segment is part of the switch II region (residues 198–215), which in $G_{t\alpha}$ is chemically coupled through Gly 198 and Gly 199 to the terminal phosphate of GTP, and whose conformation is known to undergo a major conformational rearrangement upon binding GTP from altered proteolysis[9,25,26], from fluorescence changes of the $\alpha 2$ residue Trp207 (ref. 27), and from the structures of activated and unactivated Ras[17]. We speculate with appropriate caution that the change in $\alpha 2$ and the $\alpha 2/\beta 4$ loop can be propagated to the abutting C-terminal residues 343–349 through direct interactions, thereby coupling the nature of the bound nucleotide to the specific affinity between G_α and its cognate receptor.

Receptor catalysed GDP/GTP exchange. $G_{t\alpha}$, Ras and EF-Tu differ in their affinity for guanine nucleotides. Exchange factors accelerate nucleotide exchange in both EF-Tu[28] and Ras[29], but a significant basal exchange rate persists in their absence. Exchange does not occur for transducin in the absence of activated rhodopsin. The structural feature that distinguishes $G_{t\alpha}$ from both Ras and EF-Tu is the large helical domain that forms

one wall of the nucleotide-binding cleft and thereby occludes the nucleotide. Activated rhodopsin probably opens the nucleotide-binding cleft.

The stereochemical links between the receptor-binding surface and the elements that clamp the nucleotide in the receptor-free heterotrimeric G_αs are highlighted in Fig. 3a and c. In addition to the previously described C-terminal peptide, a second peptide spanning $G_{t\alpha}$ residues 311–329 has also been shown to bind to photoactivated rhodopsin by competition assays[19]. Residues 320–323 of this peptide contribute directly to nucleoside binding through a van der Waals contact with the guanine ring. This segment is stereochemically linked to the nucleotide-binding cleft as illustrated in Fig. 3a and c, and presumably modulates nucleotide affinity in a receptor-regulated fashion.

In addition to the conserved nucleoside-binding elements of the GTPase domain, the present structure now shows the unique contributions to nucleotide binding and most likely to receptor-regulated exchange that arise from the helical domain (Fig. 3c). These binding contacts are structurally interdependent so that a receptor-triggered structural change can initiate a cooperative unravelling of the interactions that secure the nucleotide. Following release of GDP, GTP binds to the open nucleotide-binding cleft. As already described, the newly bound γ-phosphate initiates a conformational change in the switch II region. This potentially alters the structure of the abutting C-terminal 5–10 residues, ultimately leading to dissociation from photoactivated rhodopsin and the $\beta\gamma$ heterodimer.

Effector activation

$G_{t\alpha} \cdot$ GTP binds and activates cGMP–PDE by displacing the enzyme's inhibitory γ-subunits[7]. Two separate studies implicate the G_α surface loops ($\alpha2/\beta4$, $\alpha3/\beta5$ and $\alpha4/\beta6$) in effector binding and activation. All of these loops form a contiguous patch of exposed residues (Fig. 4a). Peptides designed to mimic the $\alpha3/\beta5$ loop and the $\alpha4/\beta6$ loop associate strongly with PDE-γ. In addition, the $\alpha4/\beta6$ loop peptide activates cGMP–PDE[30]. Work with $Gs\alpha/Gi\alpha$ chimaeras also establishes a critical role for all three loops in the control of adenylyl cyclase activity[31]. The crystal structure of $G_{t\alpha} \cdot$ GTPγS suggests how GTP might induce a structural change in these three effector-binding loops. The crystal structure also provides a structural basis for a recently implicated fourth effector binding region of $G_{t\alpha}$ (J. Mills et al., manuscript in preparation).

Structural consequences of GTP binding. A change in proteolysis sensitivity indicates that the switch II region (residues 198–215) undergoes a distinct transition, probably from a flexible structure to a well ordered helix upon binding GTP. Two $\alpha2$ residues, Arg 204 and Trp 207, are protected from tryptic[25] and chymotryptic[26] hydrolysis, respectively, in the $G_{t\alpha} \cdot$ GTPγS complex but not in the $G_{t\alpha} \cdot$ GDP complex. Moreover, GTP/GDP exchange alters the fluorescence of Trp 207. Trp 207 of the switch II region is coupled to the γ-phosphate through the peptide between two glycine residues, both of which are conserved in the heterotrimeric G-protein family; the backbone amide nitrogen of the mutationally sensitive Gly 199 (ref. 32) contacts the γ-phosphate while the carbonyl of that peptide (Gly 198) accepts a hydrogen bond from the heterocyclic —NH— of Trp 207. Thus, the first two turns of $\alpha2$ are stabilized by interaction with the γ-phosphate. This tandem of conserved glycines may provide the necessary freedom for a potential conformational change in $\alpha2$ upon loss of these interactions with the γ-phosphate. In addition, we predict that in the GDP-bound state the negative side chain of Glu 203 (like Asp 86 of EF-Tu–GDP[13–15]) will occupy the positively charged pocket vacated by the γ-phosphate and will be expelled upon GTP binding.

The GDP/GTP-induced changes in $\alpha2$ provide a direct link to changes in the $\alpha2/\beta4$ loop. These changes can, in turn, be transmitted to $\alpha3$ and $\alpha4$ through a series of ionic and van der Waals contacts (Fig. 4b). These interhelical contacts provide a contiguous link between the direct effect of the GTP's γ-phos-

phate on the $\alpha2$ helix and the effector-binding $\alpha3/\beta5$ and $\alpha4/\beta6$ loops. Many of the structurally observed linkages pictured in Fig. 4b involve residues that are also conserved in effector-targeted heterotrimeric G proteins and are not found in Ras (Fig. 2b), which reflects the importance of these stereochemical relays in the positioning of the three effector modulating loops.
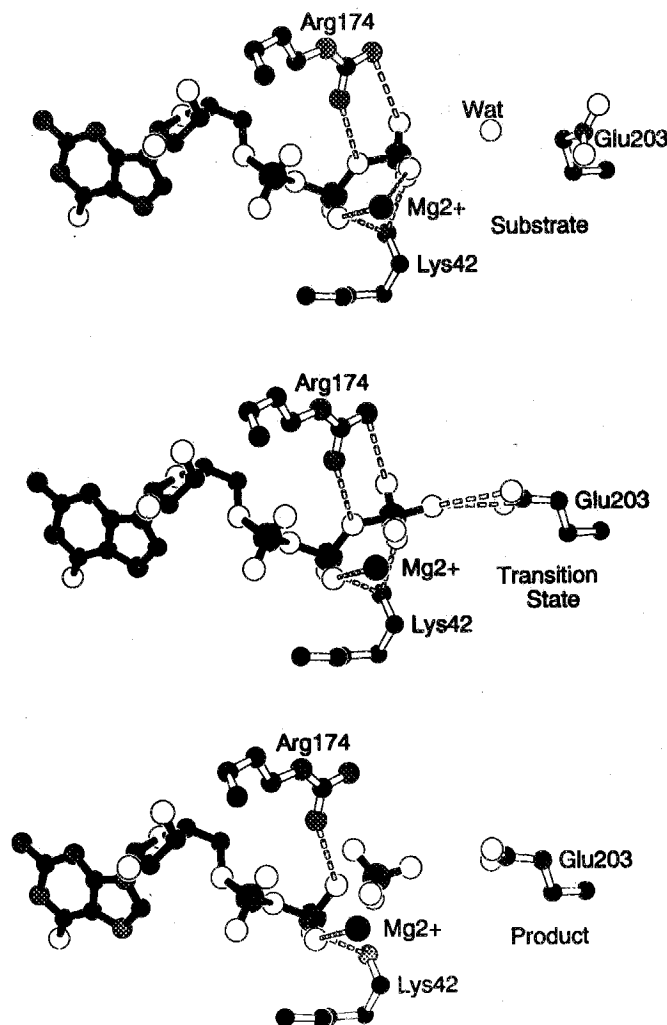

FIG. 5 Proposed catalytic mechanism for $\beta\gamma$ phosphate hydrolysis. The ground state (substrate), transition state, and products have been modelled to reflect a bound GTP rather than the catalytically resistant GTPγS. The only difference with the observed structure for the substrate is the P–S bond which has been shortened from 1.86 Å to 1.45 Å to reflect a typical P–O bond length. The active site water molecule in the ground state is situated directly in-line wth the γ-phosphate, but positioned 3.9 Å away from the phosphorus. This distance is the result of packing constraints imposed on the system by the bulky sulphur atom of the bound inhibitor (van der Waals radii is 1.7 Å versus 1.35 Å for oxygen). In the transition state, the oxygen atom of the crystallographically observed active site water has been moved to within bonding distance of the γ phosphorus. Rotation of Glu 203's Cβ–Cγ bond places its carboxylate in an ideal position to activate the water molecule by proton abstraction (general base catalysis). In addition, the interactions of the pentacoordinated phosphate with Lys 42, Arg 174 and Mg^{2+} serve to neutralize the negative charge developed in the transition state leading to enhanced catalysis through transition state stabilization. In the last step of the reaction (product), the bond between the γ-phosphorus and the bridging oxygen breaks leading to the release of a free phosphate and GDP. The likelyhood of a glutamate-activated water molecule serving as the attacking nucleophile in nucleotide hydrolysis has been suggested by Steitz[52].

The I2/α2/phosphate-binding loop linkage. One of the most striking stereochemical features of the $G_{t\alpha} \cdot GTP\gamma S$ structure are the salt bridges that link I2 (residues 226–239) to both the phosphate-binding region (residues 36–43) and α2 (Fig. 4c). These linkages probably make the position of an acidic cluster of side chains in the I2 segment (Asp 233, Asp 234 and Glu 235) sensitive to the presence or absence of the nucleotide's γ-phosphate. We speculate that this acidic patch as well as residues Glu 306, Asp 311 and Glu 314 (ref. 33) form an interface involved in binding the highly basic region of the γ-subunit of cGMP–PDE. A peptide corresponding to residues 232–259 binds PDE-γ (J. Mills et al., manuscript in preparation). The sequence variability at positions corresponding to Asp 234 and Glu 235 in the heterotrimeric family of α-subunits suggests that this surface can provide specificity in effector interactions. On the other hand, conservation of the ionic linkages to the switch II region reflects an important stereochemical connection between GTP binding and potential conformational changes in the I2 region (Fig. 2b).

GTP hydrolysis

There are two features in this crystal structure relevant to GTP hydrolysis that are not found in the structures of the stable GTP-analogue complexes of Ras[12] and EF-Tu[13]. The first is conserved arginine residue (Arg 174) that contacts the γ-phosphate directly. The second is a candidate for the general base (Glu 203) that triggers the hydrolytic attack. Arg 174 provides hydrogen bonds to the α- and γ-phosphates and the oxygen bridging the β- and γ-phosphates. These direct contacts are positioned to stabilize the negative charge that develops in the presumed pentacovalent transition state and thereby facilitate the release of the γ-phosphate from the oxygen bridging the β- and γ-phosphates (Fig. 5). Mutations of the corresponding arginine in $G_{i\alpha}$ (ref. 34) and $G_{s\alpha}$ (ref. 35) dramatically reduce their respective GTPase activities and constitutively activate their respective target effectors. Also, the guanidino group of this arginine is the target for ADP-ribosylation by cholera toxin, which blocks hydrolysis[18].

A water molecule is identically positioned to serve as a nucleophile for a direct in-line attack on the γ-phosphate in all three crystallographic representations of the $G_{t\alpha} \cdot GTP\gamma S$ complex (Fig. 5). This fixed water site is located in the corresponding position in the high-resolution structure of $Ras \cdot GMP.PNP$[12] and $EF-Tu \cdot GMP.PNP$[13]. It is likely that this water molecule has a nucleophilic role in the GTPase mechanism, but the structure of Ras has not identified the general base that activates it. In the recently described structure of EF-Tu[13], a histidine corresponding to Gln 61 in Ras or Gln 200 in $G_{t\alpha}$, is proposed to move after EF-Tu binds the ribosome in such a way that it is positioned to act as a general base. Although the mutational sensitivity of a corresponding glutamine in Ras and in G_α subunits implicates it in the GTPase mechanism, this structure and that of Ras offer little in the way of a structural explanation. In $G_{t\alpha}$, the side-chain carboxylate of Glu 203 is situated so that a rotation of its Cβ–Cγ bond places the negatively charged carboxylate in a position to abstract a proton and thereby activate the water (Fig. 5). This glutamate is well conserved across the large family of G_α subunits, which, coupled with our structural information, underscores its functional importance in heterotrimeric G-protein α-subunits (Fig. 2b). Whereas a corresponding acidic residue is absent in the smaller GTPases such as Ras, Glu 63 in the disordered α2 region of Ras (Asp 86 in EF-Tu), corresponding to $G_{t\alpha}$ residue 202, could serve as an alternative general base. In fact, Glu 63 is a site for a GTPase-inhibiting mutation in p21[Ha-ras] (ref. 36).

Glutamate 203 resides on the α2 switch helix of $G_{t\alpha}$ and is homologous to α2 of Ras[17] and EF-Tu[13], whose conformations are also sensitive to the presence or absence of the γ-phosphate. It is interesting to note that most heterotrimeric α-subunits possess a significantly higher basal GTPase rate than the small GTPases such as Ras[37]. We would argue that the higher GTPase rates in heterotrimeric G-protein α-subunits reflects (1) an inherently better-structured α2 helix, which provides a properly positioned general base without the aid of a GTPase-activating protein, and (2) the presence of a transition-state-stabilizing interaction with the side chain of a conserved arginine corresponding to Arg 174. As α2 is structurally coupled to effector binding sites, Glu 203 could be productively oriented by bound effectors[5,6].

Finally, we offer an explanation for the resistance to hydrolysis conferred by the γ-thiophosphorothioate. The bulky sulphur atom of GTPγS, identified unequivocally by its appearance in (Fo–Fc) maps and its standard phosphorus–sulphur bond distance (1.86 Å), sterically shields the phosphorus atom from a close approach by the active-site water molecule. Indeed, this prevents the side chain of Glu 203 from assuming the position needed to support in-line attack by the activated water molecule. In addition, it appears from modelling of the pentacovalent transition state that Arg 174 prevents the thiophosphate from reaching the transition state owing to a steric clash between the firmly anchored guanidino group and the equatorial sulphur atom.

In summary, this study of $G_{t\alpha} \cdot GTP\gamma S$ is a first step in developing a stereochemical context for a dynamic understanding of G-protein-coupled signal transduction through seven-helix transmembrane receptors and their cognate heterotrimeric G proteins. Until now the structural basis for experiments designed to extract structure/function correlates has been limited to that provided by other GTPases such as Ras and EF-Tu. Whereas $G_{t\alpha}$ shares many nucleotide-binding elements with the larger family of GTPases, its value as a model for G-coupled signal transduction lies in its unique structure/function relationships which are, at best, tenuously extrapolated from the models of Ras and EF-Tu. When viewed in the context of genetic, biochemical and dynamic studies on transducin and similar G-coupled systems, the present crystal structure serves as a necessary but only partial link between the functions of these G proteins and the underlying molecular mechanism by which they operate. Structural work on other complexes will complete and clarify the stereochemical picture. □

1. Conklin, B. R. & Bourne, H. R. Cell 73, 631–641 (1993).
2. Blumer, K. J. & Thorner, J. A. Rev. Physiol. 53, 37–57 (1991).
3. Tang, W. J., Krupinski, J. & Gilman, A. G. J. biol. Chem. 266, 8595–8603 (1991).
4. Berstein, G. et al. Cell 70, 411–418 (1992).
5. Arshavsky, V. Y. & Bownds, M. D. Nature 357, 416–418 (1992).
6. Stryer, L. & Bourne, H. R. A. Rev. Cell Biol. 2, 391–419 (1986).
7. Pfister, C. et al. Cell Sig. 5, 235–241 (1993).
8. Liebman, P. A., Parker, K. R. & Dratz, E. A. A. Rev. Physiol. 49, 765–791 (1987).
9. Mazzoni, M. R., Malinski, J. A. & Hamm, H. E. J. biol. Chem. 266, 14072–14081 (1991).
10. Jones, T. A. J. appl. Crystallogr. 11, 268–276 (1978).
11. Brunger, A. T. XPLOR Version 3.1 Manual Yale Univ. (1993).
12. Pai, E. F. et al. EMBO J. 9, 2351–2359 (1990).
13. Berchtold, H. Nature 365, 126–132 (1993).
14. Jurnak, F. Science 230, 32–36 (1985).
15. La Cour, T. F. M., Nyborg, J., Thirup, S. & Clark, B. F. C. EMBO J. 4, 191–212 (1985).
16. Saraste, M., Sibbald, P. R. & Wittinghofer, A. Trends biochem. Sci. 15, 430–434 (1990).
17. Milburn, M. V. et al. Science 247, 939–945 (1990).
18. Van Dop, C., Tsubokawa, M., Bourne, H. R. & Ramachandran, J. J. biol. Chem. 259, 696–698 (1984).
19. Hamm, H. E. et al. Science 241, 832–835 (1988).
20. Dratz, E. A. et al. Nature 363, 276–281 (1993).
21. Conklin, B. R., Farfel, Z., Lustig, K. D., Julius, D. & Bourne, H. R. Nature 363, 274–276 (1993).
22. Simonds, W. F., Goldsmith, P. K., Codina, J., Unson, C. G. & Spiegel, A. M. Proc. natn. Acad. Sci. U.S.A. 86, 7809–7813 (1989).
23. Gilman, A. G. A. Rev. Biochem. 56, 615–649 (1987).
24. Van Dop, C. et al. J. biol. Chem. 259, 23–26 (1984).
25. Fung, B. K.-K. & Nash, C. R. J. biol. Chem. 258, 10503–10510 (1983).
26. Mazzoni, M. R. & Hamm, H. E. J. Prot. Chem. 12, 215–221 (1993).
27. Higashijima, T. et al. J. biol. Chem. 262, 752–756 (1987).
28. Kaziro, Y. Biochem. biophys. Acta 505, 95–127 (1978).
29. Downward, J., Riehl, R., Wu, L. & Weinberg, R. A. Proc. natn. Acad. Sci. U.S.A. 87, 5998–6002 (1990).
30. Rarick, H. M., Artemyev, N. O. & Hamm, H. E. Science 256, 1031–1033 (1992).
31. Berlot, C. H. & Bourne, H. R. Cell 68, 911–922 (1992).
32. Miller, R. T., Masters, S. B., Sullivan, K. A., Beiderman, B. & Bourne, H. R. Nature 334, 712–715 (1988).
33. Artemyev, N. O. et al. J. biol. Chem. 268, 23611–23615 (1993).
34. Gupta, S. K. et al. J. molec. cell. Biol. 12, 190–197 (1992).
35. Landis, C. A. et al. Nature 340, 692–696 (1989).
36. Gibbs, J. B., Sigal, I. S. & Scolnick, E. M. Trends biochem. Sci. 10, 350–353 (1985).

37. Bourne, H. R., Sanders, D. A. & McCormick, F. Nature **348**, 125–132 (1990).
38. Kabsch, W. J. appl. Crystallogr. **21**, 67–71 (1988).
39. Kabsch, W. J. appl. Crystallogr. **21**, 916–924 (1988).
40. Otwinowski, Z. ML-PHARE CCP4 Proc. 80–88 (Daresbury Laboratory, Warrington, UK, 1991).
41. Zhang, K. Y. Acta crystallogr. **D49**, 213–222 (1993).
42. Brunger, A. T. Nature **355**, 472–475 (1992).
43. Carson, M. J. appl. Crystallogr. **24**, 958–961 (1991).
44. Robishaw, J. D., Russell, D. W., Harris, B. A., Smigel, M. D. & Gilman, A. G. Proc. natn. Acad. Sci. U.S.A. **83**, 1251–1255 (1986).
45. Nukada, T. et al. FEBS Lett. **197**, 305–308 (1986).
46. Van Meurs, K. P. et al. Proc. natn. Acad. Sci. U.S.A. **84**, 3107–3111 (1987).
47. Strathmann, M. & Simon, M. I. Proc. natn. Acad. Sci. U.S.A. **87**, 9113–9117 (1990).
48. Casey, P. J., Fong, H. K. W., Simon, M. I. & Gilman, A. G. J. biol. Chem. **265**, 2383–2390 (1990).
49. Yatsunami, K. & Khorana, H. G. Proc. natn. Acad. Sci. U.S.A. **82**, 4316–4320 (1985).
50. Capon, D. J., Chen, E. Y., Levinson, A. D., Seeburg, P. H. & Goeddel, D. Nature **302**, 33–37 (1983).
51. Laursen, R. A., L'Italien, J. J., Nagarkatti, S. & Miller, D. L. J. biol. Chem. **256**, 8102–8109 (1981).
52. Steitz, T. A. & Story, R. M. Proc. The Robert A. Welch Foundation Conference on Chemical Research XXXVI Regulation of Proteins by Ligands 173–186 (Houston, 1992).

Pulsar motion effect and Geminga's high braking index

G. S. Bisnovatyi-Kogan* & K. A. Postnov†

* Space Research Institute, Profsoyuznaya st. 84/32,
117810 Moscow, Russia
† Sternberg Astronomical Institute, Universitetskij pr. 13,
119899 Moscow, Russia

THE pulsar braking index, n, is a dimensionless quantity describing the rate at which a magnetized neutron star loses rotational energy[1]. It can be determined from pulsar timing measurements, and for distant pulsars is found to lie close to $n = 3$ (ref. 2), as predicted by theoretical models of pulsar emission mechanisms[3-5]. In contrast, the timing parameters—in particular the second derivative of the pulsation frequency—of the nearby pulsar Geminga[6-11] indicate an extremely large braking index of about 10–30. To understand this property of Geminga, we consider here the effect on the measured timing parameters of a pulsar's motion through space. We find that the Doppler effect alone can give a high apparent braking index, but only if the pulsar is very close and has an abnormally high velocity ($>$1,000 km s^{-1}). A more likely (but related) cause of the high braking index is the pulsar's proper motion: failure to correct for changes in the source coordinates with time can greatly influence the higher derivatives of the pulsar frequency, and lead to an erroneous value of n. A self-consistent analysis of the timing data, which account for both the proper motion and the Doppler effect, should permit a reliable estimate of the distance to Geminga.

The value of the pulsar braking index, n, characterizes the dependence of the energy loss of a neutron star on its angular velocity, Ω (or frequency $f = \Omega/2\pi$). Energy losses due to magnetic dipole radiation[3,4] or to stellar wind caused by the induced electrical field of the rotating magnetic dipole[5] lead to the dependence $\dot{E} \propto B^2 \Omega^4$ (where E is the rotational energy and B the surface magnetic field of the neutron star). Given that $E \propto \Omega^2$, one gets $\dot{\Omega} \propto \Omega^3$, which leads to $\ddot{\Omega}/\dot{\Omega} = 3\dot{\Omega}/\Omega$ and the canonical value of the braking index $\ddot{\Omega}\Omega/\dot{\Omega}^2 = 3$. The braking indices for most well studied pulsars are $<$3 (ref. 2). These pulsars are rather distant and their space motion does not affect significantly their braking indices. Recent X-ray[6] and γ-ray[7-10] observations of the pulsar Geminga (2CG195 + 04) and an analysis of earlier data from the COS-B satellite[11] gave the following values for frequency f_0 and its first (f_1) and second (f_2) derivatives: $f_0 \approx 4.2178$ Hz, $f_1 \approx -1.952 \times 10^{-13}$ Hz s^{-1} $f_2 = (2.8 \pm 1.6) \times 10^{-25}$ Hz s^{-2} (1σ deviation), implying that $n \approx 10$–30. To reduce this to the canonical value of the braking index, the value of f_2 would need to be an order of magnitude smaller, that is, $f_2^* = 3f_1^2/f_0 \approx 2.7 \times 10^{-26}$ Hz s^{-2}.

A pulsar's motion in space could potentially influence the observed timing parameters f_0, f_1 and f_2 in two ways. The first effect is the well known Doppler effect. The second effect arises when the pulsar's source coordinates (used for making the bary-

centric correction) are incorrect, for example, when they have been measured only once and no information about the proper motion of the source has subsequently been obtained. The second derivative of the frequency, f_2, is particularly sensitive to the accuracy of the source coordinates.

Consider the influence of the space motion on the braking index in more detail, beginning with the Doppler effect. Let a pulsar with proper frequency $\hat{f}$ move with respect to the Earth with a velocity v at a distance l. Then the observed pulsar frequency f is

$$f = \hat{f}\left(1 + \frac{v}{c}\cos\theta\right) \tag{1}$$

where c is the speed of light and θ is the angle between the pulsar velocity and the direction of propagation of the radiation in the observer's frame. Expanding $\hat{f}(t)$ and $f(t)$ to the second order $\hat{f} = \hat{f}_0 + \hat{f}_1 t + \frac{1}{2}\hat{f}_2 t^2$ and differentiating with respect to time t, one gets

$$f_0 = \hat{f}_0\left(1 + \frac{v}{c}\cos\theta\right) \tag{2}$$

$$f_1 = \hat{f}_1\left(1 + \frac{v}{c}\cos\theta\right) - \hat{f}_0\frac{v^2}{cl}\sin^2\theta \tag{3}$$

$$f_2 = \hat{f}_2\left(1 + \frac{v}{c}\cos\theta\right) - 2\hat{f}_1\frac{v^2}{cl}\sin^2\theta$$

$$- 3\hat{f}_0\frac{v^3}{cl^2}\sin^2\theta\cos\theta \tag{4}$$

For realistic values of v, the term in brackets has little effect on the values of frequency and its derivatives, and we will therefore put it equal to unity. The apparent first derivative f_1 always becomes more negative due to pulsar motion, even if the pulsar has constant proper frequency, as was first noted by Shklovskij[12]. In contrast, the second derivative f_2 will be increased by the Doppler effect if the pulsar moves away from the observer ($\cos\theta < 0$). For typical values of $v/c \approx 10^{-3}$ (that is, for pulsar velocities of $\sim$300 km s^{-1}) and adopting the measured Geminga values for $\hat{f}_1$ and $\hat{f}_2$, the second term in equation (4) is much less than the third; but both make the apparent value of f_2 higher.

The observer measures an apparent braking index

$$n = \hat{n}\frac{1 + \frac{2}{\hat{n}}\left(\frac{2\tau_d v}{l}\right)\left(\frac{v}{c}\right)\sin^2\theta - \frac{3}{\hat{n}}\left(\frac{2\tau_d v}{l}\right)^2\left(\frac{v}{c}\right)\sin^2\theta\cos\theta}{\left[1 + \left(\frac{2\tau_d v}{l}\right)\left(\frac{v}{c}\right)\sin^2\theta\right]^2} \tag{5}$$

where $\tau_d \equiv -f_0/2f_1$ is the pulsar dynamical age and $\hat{n}$ is the true braking index defined in terms of $\hat{f}_1$. If the proper values of $\hat{f}_1$ and $\hat{f}_2$ are so small that only the second term in equation (3) and the third term in equation (4) are significant, the apparent

663